Water Environment Federation
the water quality people™

Application of eco-friendly multifunctional porous graphene oxide for adsorptive sequestration of chromium in aqueous solution

Cynthia S. Nkutha ,[1] Paul N. Diagboya ,[1] Fanyana M. Mtunzi ,[1] Ezekiel D. Dikio [2]

[1] Department of Chemistry, Vaal University of Technology, Vanderbijlpark, South Africa
[2] Department of Chemical Sciences, Niger Delta University, Wilberforce Island, Nigeria

Received 19 November 2019; Revised 23 January 2020; Accepted 24 January 2020

Correspondence to: Paul N. Diagboya, Department of Chemistry, Vaal University of Technology, Vanderbijlpark, South Africa.
Email pauldn2@yahoo.com

DOI: 10.1002/wer.1303

Abstract

Graphene oxide (GO) was functionalized using two silanes ((3-aminopropyl)-triethoxysilane and (3-mercaptopropyl)-triethoxysilane) to obtain, separately, the eco-friendly amine-functionalized GO (GONH) and thiol-functionalized GO (GOSH). Both silanes were also used together to obtain the amine–thiol dual-functionalized GO (GOSN). Various physico-chemical characterizations were obtained including spectra from using Fourier-transform infrared (FTIR) spectrometer, thermogravimetric analyzer, and X-ray diffractometer. The adsorbents were used for a comparative study of Cr adsorption from aqueous solution. The obtained data were fitted to pseudo-first order (PFO) and pseudo-second order (PSO) models, the homogeneous fractal pseudo-second order (FPSO), and the Weber–Morris intraparticle diffusion (IPD) kinetics models. Model parameters of the Langmuir and Freundlich adsorption isotherm models, as well as the thermodynamics, were calculated. Characterization results showed successful functionalizations. The GONH, GOSH, and GOSN exhibited alkaline, acidic, and neutral pH, respectively, in water. Amine and thiol functional groups were observed in the new adsorbents, as well as reduced orderliness. The adsorbents had higher density per unit weight and better thermal stability than pristine GO. Equilibrium Cr adsorption was attained within 60 min for all adsorbents. The PSO and FPSO described the rate data better. The Cr adsorption decreased as solution pH increased; optimum adsorption was recorded at pH 2. Equilibrium adsorption data fitted the Langmuir adsorption isotherm model for the GONH, while it fitted the Freundlich for both GOSH and GOSN. The adsorption process was theoretically exothermic process that was spontaneous processes. The Cr adsorption capacities of these adsorbents are 114, 89.6, and 173 mg/g for GONH, GOSH, and GOSN, respectively, and these were better than several reported graphene-based adsorbents and suggest the potential of these adsorbents for water treatment. © 2020 Water Environment Federation

Practitioner points

- Graphene oxide was mono and dual-functionalized with amine and thiol groups for Cr adsorption.
- The adsorption capacities of these adsorbents were better than several earlier reported.
- These adsorbents may be used for real contaminated water treatment.

Key words

adsorption; amine and thiol-functionalized graphene oxide; chromium; equilibrium models; water treatment

1 | Introduction

The recent unprecedented industrial activities, such as metals mining over the past 7 decades, have led to the release of very high amounts of toxic pollutants into the water bodies, causing pollution in several countries (Vu et al., 2017; Wang et al., 2015). China and South Africa are two prominent countries with highly polluted water resources, but South Africa is unique due to its limited water sources and frequent droughts. Hence, technologies for removal of toxic pollutants from water cannot be over emphasized.

Pollutants of environmental concern include toxic metals, pesticides, pharmaceuticals, persistent organic pollutants, and emerging contaminants. Notable toxic metals released into water sources are Pb(II), Hg(II), As(III)/(VI), Cd(II), and Cr(III)/(VI) (Fan, Luo, Sun, & Qiu, 2012; Mohubedu, Diagboya, Abasi, Dikio, & Mtunzi, 2019; Onkani et al., 2020; Wang et al., 2015); among these, Cr is particularly ubiquitous because it features in several uses such as in stainless steel and noniron alloys, electroplating, development of pigments, leather processing, and chemicals (Kera, Bhaumik, Pillay, Ray, & Maity, 2018; Li et al., 2013). Chromium has two main oxidation states, Cr(III) and Cr(VI); the latter has high solubility and mobility in the environment and is a well-known toxin (above its maximum permissible limit of 0.1 mg/L) to biota passing through cell membranes easily and considered carcinogenic and teratogenic (Kera et al., 2018; Vu et al., 2017). Thus, the elimination of Cr in water is vital.

Various techniques have been studied for the removal of toxic metals, especially Cr, in aqueous solutions, and these include membrane systems, electrochemical reduction/precipitation, ion exchange process, and adsorption processes (Diagboya & Dikio, 2018b; Ge & Ma, 2015; Jabeen et al., 2011; Yang et al., 2014; Zhao et al., 2016). Among these, adsorption-based processes are choice techniques due to several techno-economic and environmental advantages such as low-cost and abundance of adsorbents, little need for expert knowledge or training, and environmental friendliness of the process. These advantages notwithstanding most adsorbents have inherent flaws which limit their use, such as low values of porosity, surface area and stability, as well as low adsorption capacities.

Advancements in graphene chemistry suggest it could be useful in mitigating several of the above challenges in water treatment processes. Graphene is a single-layer sheet sp^2-bonded carbon atoms arranged in honeycomb crystal lattice. It has several attractive properties for water treatment including a high theoretical specific surface area of about 2,600 m^2/g and the possibility of adding several functional groups to the large surface area via chemical functionalization (Diagboya, Olu-Owolabi, & Adebowale, 2015; Diagboya, Olu-Owolabi, Zhou, & Han, 2014b; Li et al., 2013; Vu et al., 2017; Wang et al., 2015). In fact, virtually any desired active functional group may be incorporated into the sheet. The active functional groups work in synergy with the base graphene material resulting in highly efficient adsorbent with superior structural and functional properties in comparison with the pristine graphene or its oxide. In addition, functionalization eliminates two major disadvantages observed in the pristine graphene and its oxide; they are very difficult to separate from water, and the individual graphene nanosheets easily aggregate when dried.

With the aforementioned in mind, the aim of this work was to synthesize and carry out comparison of single- and dual-functionalized graphene oxide adsorbents for Cr adsorption from aqueous solution. The active functional materials for the functionalization are (3-aminopropyl)-triethoxysilane and (3-mercaptopropyl)-triethoxysilane; these will be used separately for single functionalization and then combined in the dual functionalization. The data obtained from these adsorption studies will be explained using various adsorption models. Since it is possible for Cr to change from oxidation state of (VI) to (III) and vice versa, we have determined total chromium in this study and represented the contaminant as "Cr" throughout this work.

2 | Materials and Methods

2.1 | Synthesis of single- and dual-functionalized amino and/or thiol graphene oxide

Chemicals used for this study include natural flake graphite, potassium dichromate, potassium permanganate, hydrogen peroxide, (3-aminopropyl)-triethoxysilane (APTES), (3-mercaptopropyl)-triethoxysilane (MPTES), potassium dichromate ($K_2Cr_2O_7$), sulfuric acid, and sodium nitrate. All chemicals were of analytical grade and used with no treatment.

The exfoliation of natural flake graphite was used to prepare the graphene oxide (GO) following the modified Hummer's method as reported earlier (Diagboya, Olu-Owolabi, Zhou, et al., 2014b) which comprised of oxidation of graphite using reagents such as sodium nitrate, sulfuric acid, potassium permanganate, and hydrogen peroxide in sequence. This was followed by washing of the obtained GO in multi-cycle purification centrifugation process. Amino-functionalized GO (GONH) and thiol-functionalized GO (GOSH) were synthesized following reported method (Diagboya, Mmako, Dikio, & Mtunzi, 2019; Iqbal, Katsiotis, Alhassan, Liberatore, & Abdala, 2014) by dispersing the GO in toluene containing 2% vol. of APTES or MPTES, respectively. The mixture was then refluxed for 3 hr at 100°C and cooled to room temperature, and the GONH and GOSH adsorbents were filtered, dispersed in toluene by sonication (5 min) in order to remove any adsorbed reagents, then washed twice with ethanol, vacuum filtered, and dried at 60°C for 2 hr. The amino- and thiol (dual)-functionalized GO (GOSN) synthesis followed the similar processes as above with the exception that 2% volume each of both APTES and MPTES were added into the dispersing toluene. The schematics of these syntheses are shown in Figure 1.

The pH values of GO, GONH, GOSH, and GOSN adsorbents in H_2O and 1.0 M KCl were determined while the instrumental characterizations using Fourier-transform infrared (FTIR) spectrometer (Spectrum Two, Perkin Elmer Instruments, USA) analysis for functional groups, thermogravimetric analysis (Perkin- Elmer TGA 4000, Perkin Elmer Instruments, USA) for thermal stability, and X-ray diffractometry (XRD-7000, Shimadzu, Japan) for phase analysis.

2.2 | Chromium adsorption studies and data management

The chromium adsorption experiments were carried out using GONH, GOSH, and GOSN. Potassium dichromate ($K_2Cr_2O_7$) was used to prepare the Cr(VI) stock solution of 1,000 mg/L from which working solutions were prepared. Effects of various

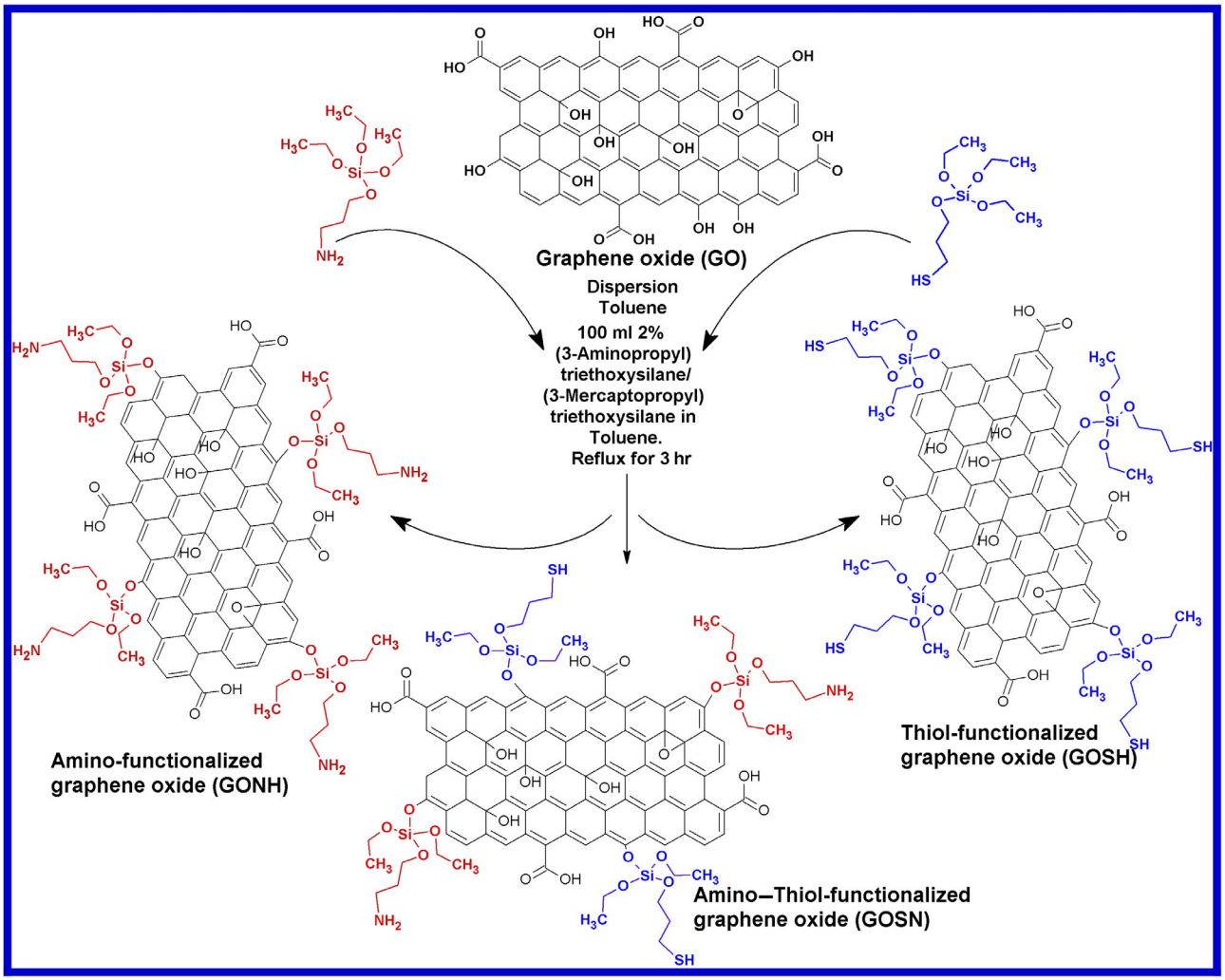

Figure 1. Schematics of the amine, thiol, and amine–thiol multifunctional graphene oxide synthesis.

operating parameters [time (5–360 min), pH (2–10), initial Cr concentrations (30–85 mg/L), and temperature (16–36°C)] were carried out. Except for the effect of time experiments, the equilibrium time used was 360 min, while 150 mg/L of Cr was employed for all experiments with the exception of the effect of initial Cr concentration experiments. A typical adsorption experiment was carried out in replicate by taking ≈10 mg of either adsorbent and 20 ml of predetermined chromium solution into 50 ml polyethylene centrifuge bottles. The mixtures' pH values were adjusted appropriately using either 0.1 M HCl or NaOH solution prior to incubation in an orbital shaker at 150 rpm until equilibrium was attained and the mixture centrifuged at 1792 *g* for 5 min. The amount of total chromium remaining in solution was determined using flame atomic absorption spectrophotometer (Shimadzu AA-7000 Japan).

The chromium adsorbed per gram of adsorbent (q_e) was calculated using the equation $q_e = (C_O - C_e)V/m$, where the initial and final total chromium concentrations (mg/L) are C_o and C_e, while the adsorbent mass and chromium solution volume are m (g) and V (ml), respectively. The data for chromium adsorption rate were described by fitting to various kinetic models such as the nonlinear Lagergren (Ebelegi et al., 2019) pseudo-first order (PFO) model $[q_t = q_e(1 - e^{-k_1 t})]$, pseudo-second order (PSO) model $[q_t = (q_e^2 k_2 t)/(1 + q_e k_2 t)]$, the homogeneous fractal pseudo-second order (FPSO) model (Olu-Owolabi et al., 2018) (Equation 1), and the Weber–Morris (Weber & Morris, 1963) intraparticle diffusion (IPD) (Equation 2);

$$q_t = \frac{k_f q_e^2 t^{\alpha}}{1 + k_f q_e t^{\alpha}} \tag{1}$$

$$q_e = k_{IPD} t^{1/2} + C \tag{2}$$

where q_t and q_e are the amounts of chromium adsorbed (mg/g) on each adsorbent at time t and equilibrium, respectively, while k_1 (/min), k_2 ($g^{-1}\ g^{-1}\ min^{-1}$), k_{IPD} ($g/g\ min^{1/2}$), and k_f are the rate constants of the PFO, PSO, FPSO, and IPD, respectively, and C (mg/g) is the amount of chromium on adsorbent surface.

The nonlinear adsorption isotherm model equations of the Langmuir (Langmuir, 1916) $\left[q_e = (Q_O b C_e)/(1 + bC_e)\right]$ and

Freundlich (Freundlich, 1906) $\left[q_e = k_f C_e^n\right]$ were employed in describing the equilibrium data, where Q_o, b, k_f, and n are the maximum adsorption capacity per unit weight, Langmuir energy-related parameter, Freundlich model adsorption constant, and isotherm linearity parameter, respectively. The OriginPro 8 software was employed in generating all model parameters.

The equilibrium constants were obtained from $K_C = q_e/C_e$, while the Equations 3 and 4 were used to obtain the thermodynamic enthalpy change ($\Delta H°$), entropy change ($\Delta S°$), and Gibbs free energy ($\Delta G°$).

$$LnK_C = \frac{\Delta S°}{R} - \frac{\Delta H°}{RT} \tag{3}$$

$$\Delta G° = -RT\mathrm{Ln}K_C \tag{4}$$

3 | Results and Discussion

3.1 | Physical and chemical characterizations

The schemes for the synthesis of the amine, thiol, and amine–thiol multifunctional graphene oxide (Figure 1) depict the covalent grafting of either or both the APTES and MPTES via the less hydrolytically stable bond (H_3C–O) onto the hydroxyl groups of the GO sheet. The pH of these adsorbents in both ultrapure water and 1 M KCl solution (Table 1) exhibited marked variations compared to the pristine GO with average pH of 2.3. The GONH, GOSH, and GOSN exhibited pH values of approximately 9.4, 3.2, and 7.1 indicating alkaline, acidic, and neutral adsorbents, respectively; the pH variations in both ultrapure water and 1 M KCl solution are within a ±0.5 value except the GOSN with 0.9 value. The neutral pH of the GOSN indicated that the functionalization of the GO by both silanes (APTES and MPTES) was successful and that the presence of these functional groups in the GOSN adsorbent canceled out the respective alkaline and acidic effects of these silanes.

The FTIR spectra (Figure 2a) indicated the presence of peaks associated with the amine and mercapto silanes on the functionalized GO sheets. The reduction as well as the almost disappearance of the intense –OH group vibrations at around 3,340 cm^{-1} on the pristine GO is evidence of the success of the functionalization and indication that this was the point of attachment of the organosilanes to the GO sheets. Several new peaks were observed in the adsorbents at around 2,930, 2,545, 1,020, and 685 cm^{-1}, and these have been ascribed to vibrations from the CH_2–CH_2 (Iqbal et al., 2014), the mercapto –SH group, the silanol stretching vibrations Si–O–Si (Diagboya, Olu-Owolabi, & Adebowale, 2014a; Iqbal et al., 2014), and the out-of-plane C–H bending vibrations (Shawabkeh, 2004) of the functional silane moieties, respectively. The peaks at 1,649 cm^{-1} for the GONH and GOSN adsorbents were ascribed to the amide I (C = O) and II (C–N) vibrations from the amino silane moiety and the GO (Diagboya et al., 2015; Iqbal et al., 2014). The intensities of these peaks at 1,649 cm^{-1} were low in the adsorbents when compared with the pristine GO; this implied that the functionalization had a shielding effect on these groups in the adsorbent.

Table 1. Some physicochemical properties of the synthesized adsorbents

ADSORBENT	PH IN WATER	PH IN 1 M KCL
GO	2.3 ± 0.1	2.4 ± 0.4
GONH	9.2 ± 0.2	9.7 ± 0.1
GOSH	2.9 ± 0.2	3.4 ± 0.0
GOSN	6.6 ± 0.1	7.5 ± 0.3

The X-ray diffractogram (Figure 2b) exhibited the characteristic intense $2\theta = 12°$ peak of the pure GO, accompanied by a weak broad peak at $2\theta = 23°$, which are indications of polar oxygen-containing functional groups formed during the exfoliation of graphite (Diagboya et al., 2015; Iqbal et al., 2014). The diffractogram of the functionalized adsorbents showed structural differences post-functionalization. For instance, the peak at 12° became highly suppressed or almost disappeared while that at 23° became slightly intense; this implied reduced orderliness and reduction in the quantity of free –OH groups in the new adsorbents as the silane moieties became attached to the GO at that point (Huang, Wu, Zhang, Ruan, & Giannelis, 2014; Li, Wang, Li, Ma, & Zhu, 2015). This is in agreement with the pH and FTIR results described above.

The temperature range for all TGA analysis was from 40 to 800°C, and the comparative spectra are shown in Figure 2c. It was observed that while the pristine GO lost 70% mass within the temperature range due to thermal losses of physisorbed water molecules and decomposition of the labile oxygen-containing functional groups (including –CO, –COOH, and –OH), the functionalized adsorbents lost far less, approximately 40% mass due to losses of some of the above functional groups as well as the amine and thiol groups of the organosilanes. Thus, the TGA suggested that organosilane functionalization increased the density per unit weight of the adsorbents. The DTA exhibited major thermal transitions at approximately 110, 330, and 520°C.

3.2 | Rate and kinetics of chromium adsorption

The Cr adsorption rate experiments were carried out as stated earlier, and the results are depicted in Figure 3a. Very rapid rates of Cr adsorption were observed for all adsorbents within the initial 60 min in following the trends: GONH <GOSH <GOSN, and during this time, approximately 95% of the Cr adsorption occurred. This was followed by a slower rate adsorption process (where the remaining of the adsorption occurred) which was observed at equilibrium or beyond 60 min. The driving force for the initial very rapid rates of Cr adsorption was attributed to adsorption occurring on vacant adsorption sites which were abundant at the beginning of the process leading to the high adsorption amounts and rates. The later slower adsorption rates were ascribed to Cr adsorption occurring on the few available vacant adsorption sites close equilibrium.

The Cr adsorption rate data were fitted to 4 adsorption kinetics models: the PFO, PSO, FPSO, and IPD models, and the fitting curves and model parameters are depicted in

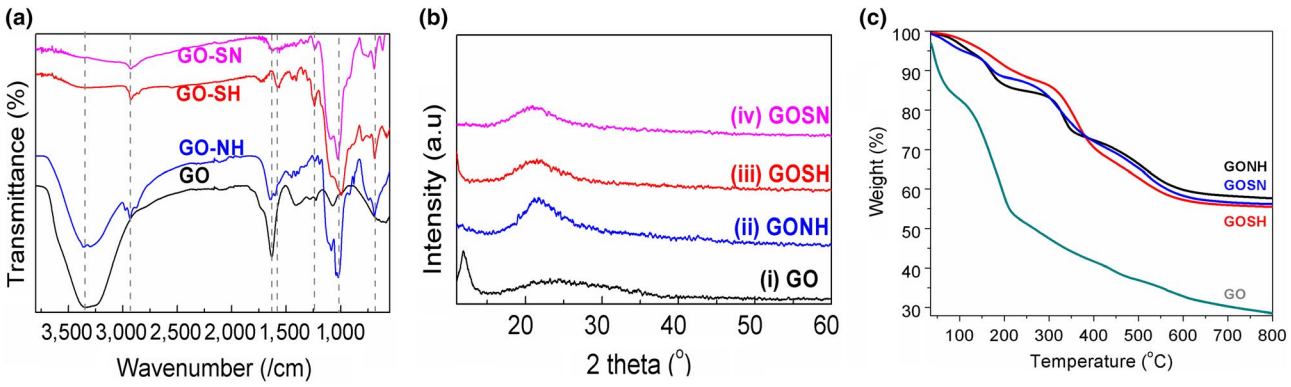

Figure 2. The synthesized GO, GONH, GOSH, and GOSN spectra for (a) FTIR; (b) XRD; and (c) TGA.

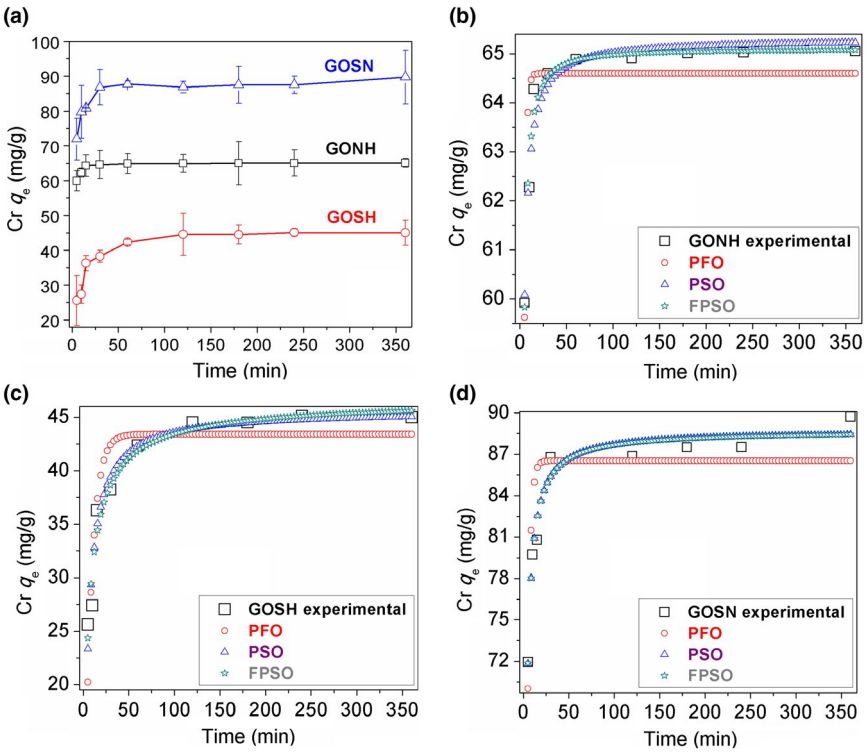

Figure 3. (a) Experimental data trend for the effect of time on Cr(VI) adsorption; fitting of the experimental data to the various kinetic models for (b) GONH, (c) GOSH, and (d) GOSN.

Figure 3b–d and Table 2, respectively. These models parameters and the experimental rate data were compared and described. A comparison of the simplistic PFO and PSO predicted q_e values to the experimentally obtained values, as well as the closeness of the correlation coefficient (r^2) values to unity, showed that the PSO model exhibited better fittings to the experimental data than the PFO. However, both models showed the same Cr rate trend and that the rate was faster for GONH than for GOSN and GOSH. The better fitting of the experimental data to the PSO suggests that Cr removal process involves electrostatic interactions between the anionic Cr species (such as $HCrO_4^-$) and the positive adsorption sites of these adsorbents (Ebelegi et al., 2019). Further comparison showed that both the PSO and FPSO exhibited similarly high q_e, k, and r^2 values and that both models could reasonably explain the adsorption data. The FPSO model parameter, k_F, confirmed the rate trend as GONH >GOSN >GOSH, as well as gave better description of the Cr adsorption. The model suggests a complex phenomenon of chemical interactions between Cr species and the chemical groups on the adsorbents sites, which involves van der Waals, hydrogen bonding, electrostatic interactions, and possibly pore-filling on the mesopores (Altenor et al., 2009; Diagboya, Olu-Owolabi, & Adebowale, 2014a).

The suggestion of pore-filling on the adsorbents mesopores by the FPSO was further tested using the intraparticle diffusion kinetic model. The model parameter C (mg/g) gives an impression of the amount of Cr adsorbed on the

Table 2. Parameters of the various kinetic models for Cr(VI) adsorption

KINETIC MODEL	PARAMETER	GONH	GOSH	GOSN
PFO	q_e (mg/g)	64.6	43.4	86.5
	k_1 (min^{-1})	0.51	0.13	0.33
	r^2	0.785	0.831	0.750
PSO	q_e (mg/g)	65.3	45.7	88.8
	k_2 (g^{-1} mg^{-1} min^{-1})	0.04	0.01	0.01
	r^2	0.957	0.946	0.963
FPSO	q_e (mg/g)	65.1	45.9	88.7
	k_f	0.02	0.01	0.01
	α	1.29	0.82	0.99
	r^2	0.967	0.946	0.957
IPD	C (mg/g)	62.2	29.1	77.7
	k_i (g/g $min^{1/2}$)	0.20	1.07	0.74
	r^2	0.372	0.659	0.532
Percent pore-filling (%)		95.7	64.5	87.6
Percent surface adsorption (%)		4.3	35.5	12.4
Experimental q_e	mg/g	65.0	45.1	88.6

Abbreviations: FPSO, fractal pseudo-second order model; IPD, intraparticle diffusion model; PFO, Pseudo-first order model; PSO, pseudo-second order model.

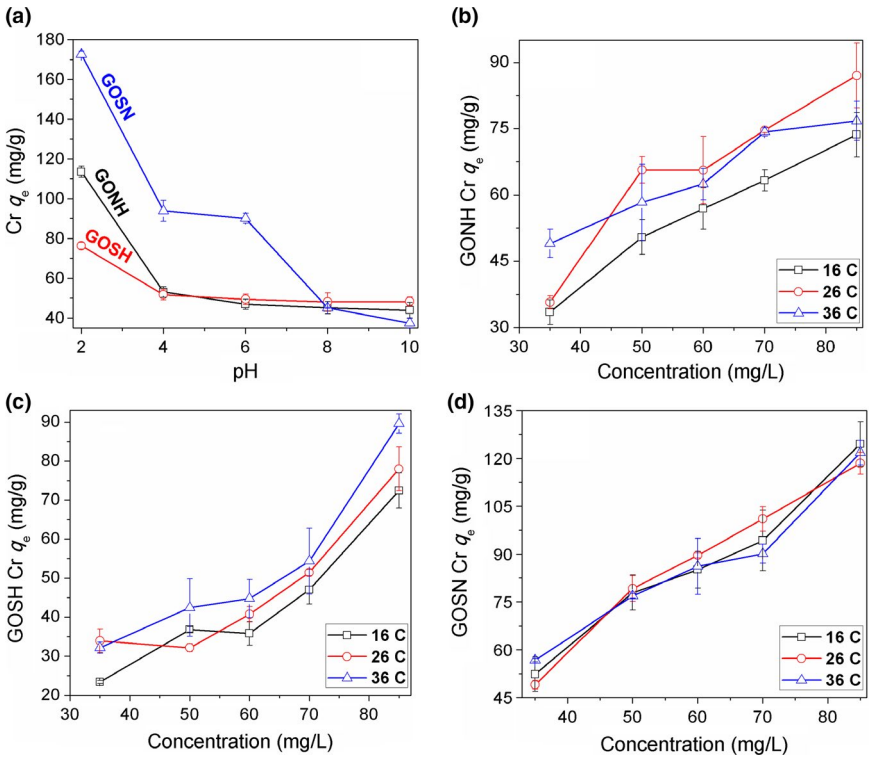

Figure 4. Cr(VI) adsorption trends at (a) varied pH; and at varying concentrations and temperatures for (b) GONH, (c) GOSH, and (d) GOSN.

adsorbent surface; if the C and q_e values are equal, it suggests that the adsorption was on the adsorbent surface, but for C value less than q_e, then the remaining amount is attributed to pore adsorption or filling (Mohubedu et al., 2019). For this study, the C values (Table 2) suggest that over 95% of Cr adsorption on the GONH occurred on the surface, compared with the 64% and 87% of GOSH and GOSN, respectively, while the rest may be attributed to pore-filling.

3.3 | Effect of pH on Cr adsorption

The ambient solution pH affects the charge density on an adsorbent and the pollutant; hence, the response of both adsorbent and pollutant to changes in the ambient solution pH is one important parameter for predicting the adsorbent's efficiency in the pollutant adsorption (Diagboya & Dikio, 2018a; Fan et al., 2012). Thus, the effect of solution pH on Cr adsorption has been examined from pH 3 to 7 and the results are depicted in Figure 4a. The trend observed revealed that the process was pH-dependent, that is, as solution pH increased, the absorption decreased. This trend was similar for all adsorbents studied; the highest Cr adsorption values were recorded at pH 2, and this was followed by sharp declines in adsorption (up to 50%) between pH 2 and 4. Beyond this point, the adsorption decrease was relatively gradual (≤5) except for GOSN which exhibited further sharp decline (up to 40% more) between pH 4 and 8; similar trend has been reported (Vu et al., 2017). This trend in Cr uptake may be described by examining the effect of solution pH on both the adsorbent and the Cr species in solution.

The rapid reduction in Cr adsorption as pH increased especially above pH 4 can be attributed to the reduced electrostatic attraction between Cr species in solution and the protonated functional groups of the GONH, GOSH, and GOSN adsorbents. This occurs because acidic pH results in the protonation of functional groups on these adsorbents as well as the species of Cr in solution (Vu et al., 2017). The stock solution for this study was prepared from a Cr(VI) salt ($K_2Cr_2O_7$); thus, the expected species of Cr in solution would be the anionic forms such as $HCrO_4^-$, CrO_4^{2-}, $Cr_2O_7^{2-}$, and $HCr_2O_7^-$. However, the dominant species would depend on the prevailing ambient pH; the $HCrO_4^-$ is predominant at low pH values (<4), while CrO_4^{2-} is dominant at pH above 7, but $Cr_2O_7^{2-}$ and $HCr_2O_7^-$ exist only at high concentrations (Vu et al., 2017). At low pH, the amine groups (and other groups, to a lesser extent, such as the –OH of the carboxylic groups) on the adsorbents are protonated with resultant positive charges which electrostatically attracts the dominant $HCrO_4^-$ species (Wang et al., 2015) and possibly other anionic species, leading the high adsorption. As the ambient pH increases, deprotonation progressively sets in, the adsorbent functional groups become less positive, while the Cr species become more negative, and consequently, the electrostatic interaction gradually decreases resulting in reduced adsorption. Above pH 7, CrO_4^{2-} is the dominant species, possibly alongside other anionic species. This coupled with the facts that the functional groups are now fully deprotonated and the high concentration of competing –OH in solution lead to far lower electrostatic attraction. Thus, the high adsorption reported for these adsorbents after pH 7 has been attributed to both reduce electrostatic attractions and pore-filling on the mesopores of these adsorbents.

3.4 | Adsorption trends at varying Cr ions and temperature

The Cr equilibrium adsorption trends on the GONH, GOSH, and GOSN adsorbents are depicted in Figure 4c,d. It was observed that Cr adsorption increased in all three adsorbents as concentration increased from 30 to 85 mg/L. This same trend was observed at the various temperatures (16, 26, and 36°C) studied (Figure 4c,d). Similar trends have been reported earlier for Cr adsorption (Vu et al., 2017; Wang et al., 2015). This trend has been attributed to the tendency of adsorbates at different concentrations between the external surface adsorption sites and the internal ones (Diagboya & Dikio, 2018b); at low adsorbate concentration in equilibrium, the movement of the adsorbate between the surface and internal adsorption sites is equal, and no movement across these boundaries is significantly impermissible. However, if the adsorbate concentration is increased on the external surface, this will once more initiate movement across these boundaries resulting in the higher adsorption observed.

In order to obtain further insight into the Cr adsorption process, the equilibrium adsorption data were fitted to two equilibrium adsorption isotherm models: the Langmuir and Freundlich. The model parameters and the correlation coefficient (r^2) values calculated using the OriginPro 8® software are shown in Table 3. Comparing these parameters and the closeness of the r^2 values to unity showed that the GONH fit better to the Langmuir adsorption isotherm model, while both GOSH and GOSN best fit the Freundlich adsorption isotherm model. The varying fits of these adsorbents to different adsorption isotherm models may be attributed to the interaction between Cr species and the active functional groups. For instance, the fit of Cr adsorption onto GONH to the Langmuir model indicates that a monolayer adsorption process occurred on sites having similar energy (possibly containing the highly electronegative atoms of O or N) for the Cr species (Diagboya et al., 2019). This is in line with the IPD *C* value (Table 2) which showed that over 95% of Cr adsorption on the GONH occurred on the monolayer surface.

On the other hand, the good fits of both the GOSH and GOSN adsorbents data to the Freundlich model suggested that the Cr adsorption process occurred on dissimilar sites of varying affinities for the Cr species (Olu-Owolabi, Diagboya, Okoli, & Adebowale, 2016). This is reasonable considering the fact that these adsorbents have functional groups containing the highly electronegative atoms of O or *N* ($-COOH_2^+$ and $-NH_3^+$) as well as the thiol group having sulfur with a dissimilar electronegativity, in addition to the internal mesopores. This Freundlich model fitting results are in line with the IPD *C* values (Table 2) which predicted that only 64 and 87% of GOSH and GOSN Cr adsorption, respectively, were on the monolayer surfaces, while the rest were attributed to pore-filling.

The effect of temperature on Cr species adsorption was also ascertained; it was observed that increasing the ambient solution temperature from 16 to 36°C (Figure 4b-d) showed that Cr adsorption slightly increased as temperature rose from 16 to 26°C for all three adsorbents. However, increasing the temperature further to 36°C enhanced adsorption only on the GOSH, but uptake on the GONH was higher than at 16°C but lower than at 26°C, while for the GOSN the adsorption was lower than at 16°C. Thus, increasing temperature had different effects on Cr adsorption on these adsorbents.

Table 3. Parameters of the various adsorption isotherm models for Cr(VI) adsorption

ADSORPTION ISOTHERM MODEL	PARAMETER	GONH	GOSH	GOSN
Langmuir	Q_o (mg/g)	305	1.2×10^5	1.8×10^3
	β	4×10^{-3}	6.07	8.33
	r^2	0.986	0.811	0.960
Freundlich	n	0.82	1.39	0.94
	k_f	1.91	0.14	1.84
	r^2	0.981	0.890	0.962

Table 4. Thermodynamic parameters for Cr adsorption on GONH, GOSH, and GOSN adsorbents

THERMODYNAMIC PARAMETER		GONH	GOSH	GOSN
$\Delta H°$	kJ/mol	−70.9	−19.5	7.0
$\Delta S°$	J/mol K^{-1}	253	66.9	5.14
$\Delta G°$ (kJ/mol)	289 K	−2.91	0.35	−9.02
	303 K	−3.30	−0.91	−7.35
	310 K	−8.07	−0.96	−9.20

The effect of temperature data has been evaluated using the thermodynamic parameters ($\Delta H°$, $\Delta S°$, and $\Delta G°$), and the values are recorded in Table 4. The negative $\Delta G°$ values implied that Cr adsorption on these adsorbents at the various temperatures were spontaneous and feasible processes, while the positive $\Delta S°$ values implied that there was an increase in Cr species randomness in solution at equilibrium. The negative $\Delta G°$ value of Cr adsorption on GOSH was an exception to this trend. This was attributed to inherent errors associated with calculations of thermodynamic parameters using the linear plots when studying low energy surfaces, which could result in shifts of small or borderline values from one extreme to another. When such occurs, small negative values could shift to small positive values. The $\Delta H°$ values of the GONH and GOSH adsorbents indicated that theoretically, the adsorption process is exothermic for both adsorbents, while for the GOSN adsorbent, it was endothermic.

The adsorption capacities of all three adsorbents for Cr adsorption were compared to some graphene-based materials published in the literature (Table 5). The data from the comparison showed that the study adsorbents performed better than several graphene-based adsorbents reported for Cr adsorption, as well as pristine GO. Though Table 5 showed that pristine GO had slightly higher adsorption capacity than the GONH (Yang et al., 2014), the challenge with GO (reason for preferring the GONH) is that it is well dispersed in water and very difficult to separate unlike the denser GONH adsorbent. The proposed electrostatic interactive mechanism of the anionic Cr species adsorption on the amine and thiol groups is depicted in Figure 5.

4 | Conclusion

The amine-functionalized GO (GONH), thiol-functionalized GO (GOSH), and amine–thiol-functionalized GO (GOSN) were successfully synthesized. Due to the characteristics of the attached functional groups, GONH, GOSH, and GOSN exhibited alkaline, acidic, and neutral pH, respectively, in water. In the GOSN adsorbent, the presence of both alkaline and acidic functionalities canceled out their respective effects resulting in a neutral adsorbent. The infrared spectra showed the presence of amine and thiol functional groups in the new adsorbents,

Table 5. Comparison of Cr adsorption capacities of GONH, GOSH, and GOSN with literature

ADSORBENT	Q_E (MG/G)	REMARK	REFERENCES
Magnetite GO–alginate beads	≈7.0	Total Cr	Vu et al. (2017)
Magnetic cyclodextrin–chitosan–GO	≈67.0	Total Cr	Li et al. (2013)
GOSH	89.6	Total Cr	This study
GO	92.7	Cr(III)	Yang et al. (2014)
GONH	114	Total Cr	This study
Magnetic b–cyclodextrin/GO composite	120	Total Cr	Fan et al. (2012)
Magnetic diethylenetriamine–GO	124	Total Cr	Zhao et al. (2016)
Zero valent iron nanoparticles (nZVI)	148	Cr(VI)	Jabeen et al. (2011)
Graphene–nZVI composite	162	Cr(VI)	Jabeen et al. (2011)
GOSN	173	Total Cr	This study
Triethylenetetramine–GO–chitosan composite	220	Cr(VI)	Ge and Ma (2015)
Magnetic polypyrrole–rGO	293	Cr(VI)	Wang et al. (2015)

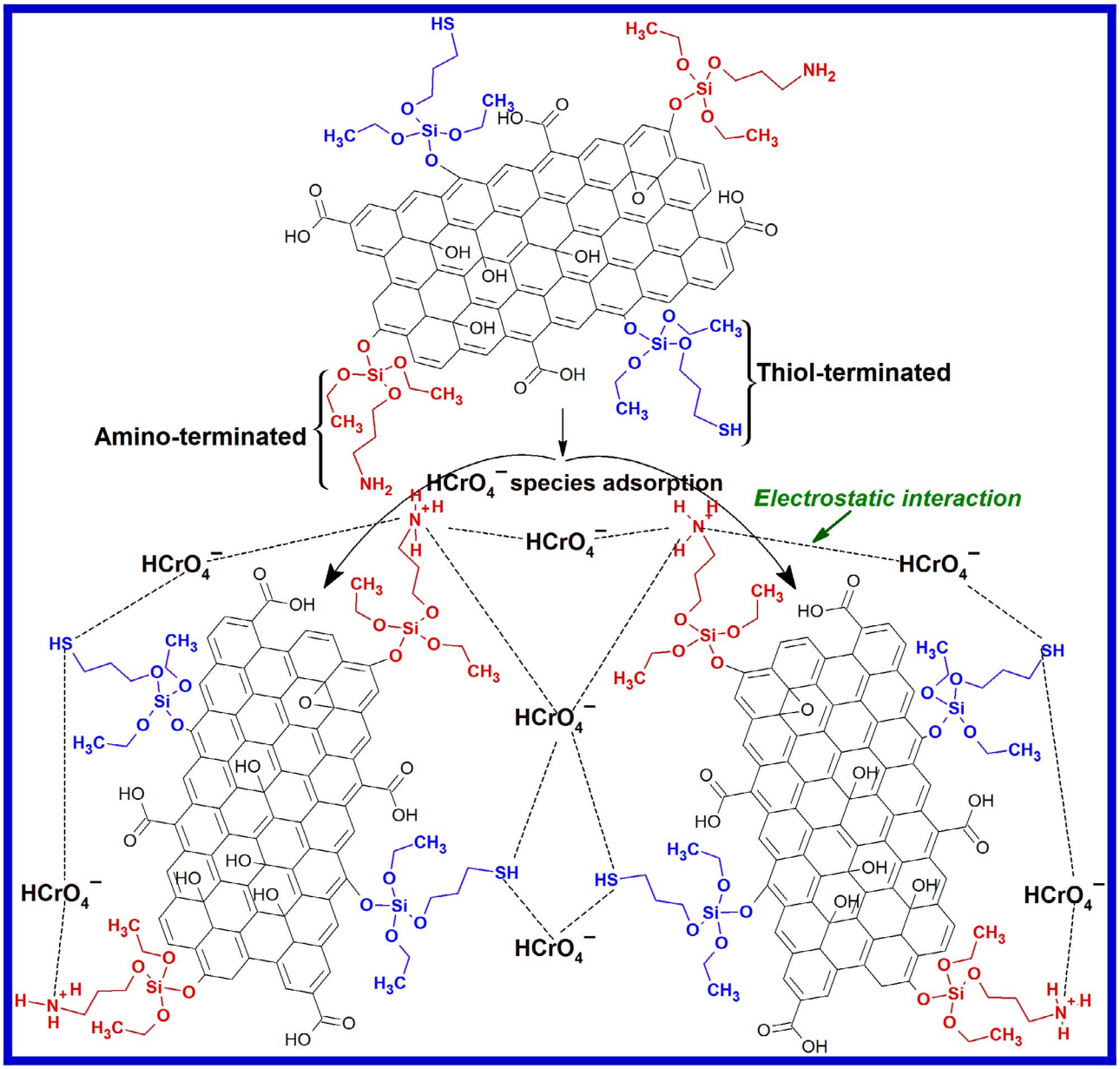

Figure 5. Schematics of the anionic Cr species adsorption on the amine- and thiol-terminated ends of the multifunctional graphene oxide adsorbents.

while the XRD implied reduced orderliness as the free –OH groups in GO were used up. These adsorbents had higher density per unit weight and better thermal stability than pristine GO.

Equilibrium Cr adsorption was fast and attained within 60 min. for all adsorbents. The rate data fitted the PSO and FPSO models implying electrostatic interactions between the anionic Cr(VI) species and the adsorption sites of these adsorbents, as well as other complex chemical interactions between Cr species and chemical groups on the adsorbents sites such as van der Waals interactions and pore-filling on the mesopores. The Cr adsorption trend was concentration and pH-dependent, increasing with concentration until maximum adsorption and decreasing as solution pH increased; optimum adsorption was recorded at pH 2. Increase in temperature had varying effects on the process on each adsorbent; as temperature rose from 16 to 26 and then 36°C, adsorption increased continuously for GOSH, while it had no significant effect for GOSN, but it initially increased and then decreased for GONH. Equilibrium adsorption data fitted the Langmuir adsorption isotherm model for the GONH, while it fitted the Freundlich for both GOSH and GOSN. These suggest Cr adsorbed as monolayer onto adsorption sites having similar energy on GONH, while the process occurred on dissimilar sites of varying affinities for the Cr species on both GOSH and GOSN adsorbents. The Cr adsorption capacities of these adsorbents are 113.5, 89.6, and 172.5 mg/g for GONH, GOSH, and

GOSN, respectively, and these were better than several reported graphene-based adsorbents.

Acknowledgments

We acknowledge the Department of Chemistry and Research Directorate, Vaal University of Technology, Vanderbiljpark, South Africa, and the SASOL Research grant (VAT Number: 4430113102). There is no known conflict of interests for these publications.

References

Altenor, S., Carene, B., Emmanuel, E., Lambert, J., Ehrhardt, J.-J., & Gaspard, S. (2009). Adsorption studies of methylene blue and phenol onto vetiver roots activated carbon prepared by chemical activation. *Journal of Hazardous Materials*, *165*, 1029–1039. https://doi.org/10.1016/j.jhazmat.2008.10.133

Diagboya, P. N., & Dikio, E. D. (2018a). Dynamics of Mercury solid phase extraction using Barbula lambarenensis. *Environmental Technology and Innovation*, *9*, 275–284. https://doi.org/10.1016/j.eti.2018.01.002

Diagboya, P. N., & Dikio, E. D. (2018b). Scavenging of aqueous toxic organic and inorganic cations using novel facile magneto-carbon black-clay composite adsorbent. *Journal of Cleaner Production*, *180*, 71–80. https://doi.org/10.1016/j.jclepro.2018.01.166

Diagboya, P. N., Mmako, H. K., Dikio, E. D., & Mtunzi, F. M. (2019). Synthesis of amine and thiol dual functionalized graphene oxide for aqueous sequestration of lead. *Journal of Environmental Chemical Engineering*, *7*(6), 103461–https://doi.org/10.1016/j.jece.2019.103461

Diagboya, P. N., Olu-Owolabi, B. I., & Adebowale, K. O. (2014a). Microscale scavenging of pentachlorophenol in water using amine and tripolyphosphate-grafted SBA-15 silica: Batch and modeling studies. *Journal of Environmental Management*, *146*, 42–49. https://doi.org/10.1016/j.jenvman.2014.04.038

Diagboya, P. N., Olu-Owolabi, B. I., & Adebowale, K. O. (2015). Synthesis of covalently bonded graphene oxide–iron magnetic nanoparticles and its kinetics of mercury removal. *RSC Advances*, *5*, 2536–2542.

Diagboya, P. N., Olu-Owolabi, B. I., Zhou, D., & Han, B.-H. (2014b). Graphene oxide–tripolyphosphate hybrid used as a potent sorbent for cationic dyes. *Carbon*, *79*, 174–182. https://doi.org/10.1016/j.carbon.2014.07.057

Ebelegi, A. N., Ayawei, N., Wankasi, D., Dikio, E. D., Diagboya, P. N., & Mtunzi, F. M. (2019). Covalently bonded polyamidoamine functionalized silica used as a Pb(II) scavenger from aqueous solution. *Journal of Environmental Chemical Engineering*, *7*, 103214. https://doi.org/10.1016/j.jece.2019.103214

Fan, L., Luo, C., Sun, M., & Qiu, H. (2012). Synthesis of graphene oxide decorated with magnetic cyclodextrin for fast chromium removal. *Journal of Materials Chemistry*, *22*, 24577–24583. https://doi.org/10.1039/c2jm35378d

Freundlich, H. M. F. (1906). Über die adsorption in lösungen. *Zeitschrift für Physikalische Chemie*, *57A*(57A), 385–470.

Ge, H., & Ma, Z. (2015). Microwave preparation of triethylenetetramine modified graphene oxide/chitosan composite for adsorption of Cr(VI). *Carbohydrate Polymers*, *131*, 280–287. https://doi.org/10.1016/j.carbpol.2015.06.025

Huang, Y.-F., Wu, P.-F., Zhang, M.-Q., Ruan, W.-H., & Giannelis, E. P. (2014). Boron cross-linked graphene oxide/polyvinyl alcohol nanocomposite gel electrolyte for flexible solid-state electric double layer capacitor with high performance. *Electrochimica Acta*, *132*, 103–111. https://doi.org/10.1016/j.electacta.2014.03.151

Iqbal, M. Z., Katsiotis, M. S., Alhassan, S. M., Liberatore, M. W., & Abdala, A. A. (2014). Effect of solvent on the uncatalyzed synthesis of aminosilane-functionalized graphene. *RSC Advances*, *4*, 6830–6839. https://doi.org/10.1039/C3RA46586A

Jabeen, H., Chandra, V., Jung, S., Lee, J. W., Kim, K. S., & Kim, S. B. (2011). Enhanced Cr(vi) removal using iron nanoparticle decorated graphene. *Nanoscale*, *3*, 3583–3585. https://doi.org/10.1039/c1nr10549c

Kera, N. H., Bhaumik, M., Pillay, K., Ray, S. S., & Maity, A. (2018). m-Phenylenediamine-modified polypyrrole as an efficient adsorbent for removal of highly toxic hexavalent chromium in water. *Materials Today Communications*, *15*, 153–164. https://doi.org/10.1016/j.mtcomm.2018.02.033

Langmuir, I. (1916). The constitution and fundamental properties of solids and liquids. *Journal of the American Chemical Society*, *38*, 2221–2295.

Li, L., Fan, L., Sun, M., Qiu, H., Li, X., Duan, H., & Luo, C. (2013). Adsorbent for chromium removal based on graphene oxide functionalized with magnetic cyclodextrin–chitosan. *Colloids and Surfaces B: Biointerfaces*, *107*, 76–83. https://doi.org/10.1016/j.colsurfb.2013.01.074

Li, X., Wang, Z., Li, Q., Ma, J., & Zhu, M. (2015). Preparation, characterization, and application of mesoporous silica-grafted graphene oxide for highly selective lead adsorption. *Chemical Engineering Journal*, *273*, 630–637. https://doi.org/10.1016/j.cej.2015.03.104

Mohubedu, R. P., Diagboya, P. N. E., Abasi, C. Y., Dikio, E. D., & Mtunzi, F. (2019). Magnetic valorization of biomass and biochar of a typical plant nuisance for toxic metals contaminated water treatment. *Journal of Cleaner Production*, *209*, 1016–1024. https://doi.org/10.1016/j.jclepro.2018.10.215

Olu-Owolabi, B. I., Diagboya, P. N., Okoli, C. P., & Adebowale, K. O. (2016). Sorption behaviour of pentachlorophenol in sub-Saharan tropical soils: soil types sorption dynamics. *Environmental Earth Sciences*, *75*(24). https://doi.org/10.1007/s12665-016-6307-9

Olu-Owolabi, B. I., Diagboya, P. N., Unuabonah, E. I., Alabi, A. H., Düring, R.-A., & Adebowale, K. O. (2018). Fractal-like concepts for evaluation of toxic metals adsorption efficiency of feldspar-biomass composites. *Journal of Cleaner Production*, *171C*, 884–891. https://doi.org/10.1016/j.jclepro.2017.10.079

Onkani, S. P., Diagboya, P. N., Mtunzi, F. M., Klink, M. J., Olu-Owolabi, B. I., & Pakade, V. (2020). Comparative study of the photocatalytic degradation of 2–chlorophenol under UV irradiation using pristine and Ag-doped species of TiO_2, ZnO and ZnS photocatalysts. *Journal of Environmental Management*, *260*, 110145. https://doi.org/10.1016/j.jenvman.2020.110145

Shawabkeh, R. A. (2004). Synthesis and characterization of activated carbo-aluminosilicate material from oil shale. *Microporous and Mesoporous Materials*, *75*, 107–114. https://doi.org/10.1016/j.micromeso.2004.07.020

Vu, H. C., Dwivedi, A. D., Le, T. T., Seo, S.-H., Kim, E.-J., & Chang, Y.-S. (2017). Magnetite graphene oxide encapsulated in alginate beads for enhanced adsorption of Cr(VI) and As(V) from aqueous solutions: Role of crosslinking metal cations in pH control. *Chemical Engineering Journal*, *307*, 220–229. https://doi.org/10.1016/j.cej.2016.08.058

Wang, H., Yuan, X., Wu, Y., Chen, X., Leng, L., Wang, H., … Zeng, G. (2015). Facile synthesis of polypyrrole decorated reduced graphene oxide–Fe_3O_4 magnetic composites and its application for the Cr(VI) removal. *Chemical Engineering Journal*, *262*, 597–606. https://doi.org/10.1016/j.cej.2014.10.020

Weber, W. J., & Morris, J. C. (1963). Kinetics of adsorption on carbon from solutions. *Journal of the Sanit. Engineering Division, American Society of Civil Engineers*, *89*, 31–60.

Yang, S., Li, L., Pei, Z., Li, C., Lv, J., Xie, J., … Zhang, S. (2014). Adsorption kinetics, isotherms and thermodynamics of Cr(III) on graphene oxide. *Colloids and Surfaces A: Physicochemical and Engineering Aspects*, *457*, 100–106. https://doi.org/10.1016/j.colsurfa.2014.05.062

Zhao, D., Gao, X., Wu, C., Xie, R., Feng, S., & Chen, C. (2016). Facile preparation of amino functionalized graphene oxide decorated with Fe_3O_4 nanoparticles for the adsorption of Cr(VI). *Applied Surface Science*, *384*, 1–9. https://doi.org/10.1016/j.apsusc.2016.05.022